SLAC-PUB-2186
August 1978
(I)

PRELIMINARY RESULTS ON TESTS OF A CERENKOV RING IMAGING DEVICE EMPLOYING A PHOTOIONIZING PWC *

S. Durkin, A. Honma, D.W.G.S. Leith
Stanford Linear Accelerator Center
Stanford University, Stanford, California 94305

ABSTRACT

A brief description of techniques and problems of ring imaging Cerenkov detectors employing photoionizing PWC's is discussed. Preliminary results on a one dimensional ring imaging device tested at SLAC in May and June of 1978 are then presented. These results include rough measurements of the Cerenkov ring in nitrogen, argon, neon and helium produced by a collimated positron beam.

(Talk presented by A. Honma at the 1978 ISABELLE Summer Workshop, Upton, New York, July 17 - 28, 1978)

* Work supported by the Department of Energy

I. Review of Ring Imaging and Detection

The recent interest in Cerenkov ring imaging has been stimulated largely by Sequinot and Ypsilantis[1] who have published several articles on the desirability and feasibility of obtaining particle velocity information through measurement of the angle of emitted Cerenkov light. In Fig. 1 it is seen that if a particle originates from the center of two concentric spheres, radius R and R/2, then the cone of Cerenkov light emitted by the particle can be focused by the outer sphere into a ring of radius r on the inner sphere. The radius of the ring on the inner sphere is given by:

$$r = f \tan \theta$$

where

f = focal length of the mirrored outer sphere = R/2

θ = Cerenkov angle.

The velocity of the particle can then be obtained from the familiar Cerenkov relation:

$$\cos \theta = 1/n\beta$$

where

n = index of refraction of the Cerenkov radiator

Assuming one has calculated the center of this imaged ring using the trajectory of the particle, each imaged Cerenkov photon represents an independent measurement of the ring's radius. Thus, the error in determining the radius r is given by:

$$\Delta r \cong \frac{\sigma}{\sqrt{N}}$$

σ = measurement error in a single photon's position

N = number of photons detected

Thus, to measure the radius well, one needs to:

1. Maximize the number of imaged photons
2. Obtain good single photon position resolution.

Figs. 2 and 3a, b, c show the ring radii and the corresponding errors of measurement one can obtain using typical detector parameters for pions, kaons, and protons. From Fig. 2 it is easily seen that one can obtain good particle identification over large momentum ranges if one has a rough initial knowledge of the momentum. Fig. 3 shows the error in momentum measurement that is obtained using typical detector parameters.

To maximize the number of detected photons, Sequinot and Ypsilantis proposed the use of photoionization detectors which have been shown to have high quantum efficiencies in the vacuum ultraviolet (VUV) region of the spectrum. Working in the VUV one can obtain a larger number of photons than with a conventional Cerenkov counter because of the larger range of detected photon energies (six to ten ev in the VUV versus a typical two to four ev in the visible). A distinct problem for imaging counters is encountered in the VUV since dispersion $\left(\frac{dn}{d\nu}\right)$ in this region of the spectrum can be very large.

The formula for calculating the number of photons detected is:

$$N = N_o L \sin^2\theta$$

where

L = length of radiator

θ = Cerenkov angle

$$N_o = \frac{\alpha}{\hbar c} \int_{E_1}^{E_2} \varepsilon_P(E)\ \varepsilon_T(E)\ \varepsilon_R(E)\ dE$$

where

ε_P = Device detection efficiency.

ε_T = Transmission efficiency of the window separating the Cerenkov radiator and detector.

ε_R = Reflectance of the spherical mirror.

E_1, E_2 = Photon energy cutoffs

Working in the VUV puts further restrictions on the detection device, namely:

1. One is forced to use H_2, N_2, or one of the noble elements, in either gaseous or liquid form, as a Cerenkov radiator because almost all substances are strongly absorbing in the VUV.
2. One must use a photoionizing agent with high quantum efficiency over a large photoionizing energy range.
3. One must construct a detector that can employ this photoionizing agent and has the position resolution desired.
4. One needs a window that transmits well in the VUV to separate the radiator (transparent to VUV) from the detector (VUV absorber).

As for the second and fourth considerations, much work has been done in these areas and Fig. 4 shows some potential photoionizing agents and some window materials and their effective photon energy cutoffs[4].

We began by constructing a prototype two dimensional readout detector. Sequinot and Ypsilantis had proposed a needle chamber (see Fig. 5) utilizing the tips of the needles to produce a strong field gradient and this strong field gradient would produce proportional avalanches when the Cerenkov

photon photoionized. We tested several configurations with needle arrays but found in each case that we were unable to achieve counting efficiencies of greater than 10% with minimum ionizing particles. We think these test configurations failed because much of the chamber active area did not focus on to the needle points but rather to the needle shafts, leaving large regions with little or no amplification. Our other attempts with wire wrap pins (with sharp edges as well as points) and with segmented wire anodes met with similar lack of success. We also investigated cathode readout pads using induced pulses from a standard proportional wire chamber. This method had excellent efficiency but suffered from the complication of very large numbers of readout channels from the pads.

Our tests showed this latter configuration was well suited for a small scale detector, so we decided to build a test device using readily available components in order to verify that ring imaging using photoionization was indeed possible with current technology.

Our goals in this study were to:

1. Observe the Cerenkov ring image, using a photoionizing PWC with anode wire readout (one dimension); then, later cathode pad readout (two dimensions) if time permitted.
2. Try various radiator gases, observing and measuring the change in ring radius and number of photons detected.
3. Measure the average O_2 absorption coefficient. This is important because strong O_2 absorption could put strict requirements on future counters.
4. Vary the pressure of the radiator gas noting change in ring

radius and number of photons.

II. SLAC Test Device and Set-Up

Table 1 summarizes some of the important parameters of our test beam and apparatus.

Table I

BEAM AND RUN PARAMETERS

Beam Parameters
3 GeV/c e^+ (SLAC test beam).
Spot size < 2 mm FWHM.
$\Delta p/p$ < 1% FWHM.
π/e contamination < 0.01.
Beam divergence $\sim$ 1 mr.
0.5 particles/pulse, 6 to 20 particles/second, 1.6 μs pulse width.
Run Parameters
Dates of runs: May and June 1978.
Radiator gases used (purtiy in parenthesis): N_2(99.996%), Ar(99.999%), Ne-He (spark chamber grade-probably 99.9%), He(99.995%).
Photoionizing detector gas: 84% Ar, 15% CO_2, 1% benzene.

Fig. 6 is a cross section of the radiator tube which shows the positions of the mirrors and detection PWC. Note that we employed a flat mirror angled to 45° to allow the ring image to be focused on a plane away from the beam to eliminate confusion with beam particles. The photoionizing PWC was placed at the focus of the spherical mirror which was 114.3 cm from the mirror. This optical arrangement resulted in an effective length of radiator gas of 96.5 cm.

Fig. 7 is a blowup of the photoionization PWC detector. The important

features are the 4 mm thick, 9.65 cm diameter LiF window, a wire weave (127 μm thick) cathode mesh plane that was pushed flush against the window, 55 anode readout wires mounted at 2 mm spacing made of 20 μ diameter gold-plated tungsten, and a polished aluminum plate for the other cathode plane. The gap spacing was 6 mm and the photoionizing agent was a 1% benzene gas fraction in an 85% argon-15% CO_2 mixture.

Due to a large amount of scattering and showering caused by the 45° mirror and the fact that the mirror mount was positioned in the beam, we found it necessary to install a large array of veto counters in order to insure that one and only one unscattered particle passed through the apparatus. The multiple scattering was large enough that we found it necessary to further define the beam with a second PWC (this one using magic gas), although upstream of the Cerenkov tube the beam spot was very small (< 2 mm FWHM). The arrangement of the beam defining counters is displayed in Fig. 8, and the trigger logic is also shown.

The data acquisition system is shown schematically in Fig. 9. An LSI-11 was used to control the CAMAC crate which contained modules that buffered the incoming data. The LSI-11 also had a serial interface to the main computer center where the data was stored on disk. The interface to the local terminal and the line to the main computer allowed on-line monitoring and full access to the main computer.

III. Results of the Test Run

Before installing the photoionizing PWC on the radiator tube, we put the PWC directly into the beam in order to obtain an efficiency plateau

with 3 GeV positrons. This curve is shown in Fig. 10a. The plateau here is very short since the last point (3.4 KV) represents the chamber breakdown threshold. Also, it should be noted that there is an 80% efficiency rise in a range of 50 v compared to 200 v for a magic gas mixture (see Fig. 10b). So, although the chamber could be run 98% efficient with 3 GeV positrons (which would ionize ~ 50 electrons in the chamber), the short plateau indicated that obtaining good single electron detection efficiency would be unlikely.

One of the great concerns with using a photoionizing proportional chamber was that the UV photons created in the PWC avalanche, or created from decay of metastables in the gas, might travel a moderate distance and then photoionize to create another nonprimary avalanche. This travel is inhibited in magic gas by the highly UV-absorbing components, but with Ar-CO_2-benzene it was unclear what the effect would be. To test this we constructed a mask which was placed next to the LiF window so that the middle 20 wires of the chamber were exposed to incoming Cerenkov photons. We then bolted the PWC into position on the upper flange of the Cerenkov radiator tube. We put iron in the beam just upstream of the tube in order to scatter the beam so that the Cerenkov light would illuminate the chamber uniformly. Fig. 11 is a histogram of the number of times a wire was hit versus the wire number for this mask test. The histogram is an accumulation of wire hits integrated over many beam particles. Argon was used as the radiator gas, and the "clustering" in the caption of the figure refers to the fact that groups of adjacent wires hit were counted as single hits at the center of mass of the "cluster." If UV "travel" was a large problem, one would expect many hits in the masked areas. The small number of hits in those areas is consistent with background (i.e.,

what would be there if we had totally masked off the window). It is important to note that avalanche quenching is nevertheless a problem since the cluster size increased as we increased the voltage. We had to lower the voltage in order to obtain better position resolution, but it was quite clear that by lowering the voltage we sacrificed the single photon detection efficiency. The masking test showed that we could run the PWC so that the avalanches were localized.

Since we were reading out the anode wires, we needed to calculate what distribution one would expect for a ring of photons imaged onto a plane of wires. In the perfect case of an infinite number of wires one gets the distribution shown in Fig. 12a. If one considers the following factors: finite number of wires, the resolution of the chamber and the spread due to uncertainty of the center of the distribution (finite beam spread), one gets a distribution with a double bump shape (see Fig. 13b). Most background contributions lead to a distribution shown in Fig. 12c, which is easily distinguishable from the expected signal.

Fig. 13 shows the integrated image of a Cerenkov ring using N_2 at 1 atm as a radiator gas. Due to poor quantum efficiency of our detector, it was necessary to integrate over many particles in order to observe a clear ring image. (For example, we integrated over 1098 particles to obtain the N_2 distribution in Fig. 13.) The "corrected" in the title refers to two corrections made on the data; one is a subtraction of background due to noise pickup and direct particle scattering into the chamber, and the other is a weighting factor for each wire due to variation in collection efficiency and amplifier gains from wire to wire. The smooth curve is a fit to the data using the following functional form;

$$f(x_i) = \int_{-1}^{1} \frac{r \exp(-a[ru - x_i + b]^2)du}{1 - u^2} = \int_{-r+x_i-b}^{r+x_i-b} \frac{\exp(-av^2)\,dv}{1 - \frac{(v - x_i + b)^2}{r^2}}$$

a = $1/(2\sigma^2)$, σ = sigma of the gaussian

b = center of ring

r = radius of ring

x_i = wire number = i

i = bin number in histogram

The function $f(x_i)$ is a composite of the perfect case functional form (as shown in Fig. 12a) and a gaussian term which incorporates the uncertainty in beam particle position, the resolution of the imaging PWC, and the uncertainty in ring radius (caused by the fact that the index of refraction varies as a function of photon energy). We fit this function to the measured data by minimizing the chi-squared given below with the MINUIT program.

$$\chi^2 = \sum_i \frac{(N_i - cf(x_i))^2}{N_i}$$

N_i = counts in bin i of histogram to be fitted

c = normalization factor

From our understanding of the resolution and beam position accuracy, we fixed the sigma of the gaussian in the function $f(x_i)$ to be equal to 2.5 wire spacings. The free parameters in the fit were the position of the center of the ring, the overall normalization factor and, most important, the radius of the ring.

It appeared that one edge of the distribution in Fig. 13 might be due to the window cutoff (the window aperture was smaller than the active area of the PWC). We demonstrated that this was not the case by observing the left edge and lobe of the ring distribution (shown in Fig. 14) which was shifted by a known amount when we tilted the radiator tube. Notice that there was very little background or other spurious signal contribution outside the ring edge.

We repeated these measurements with the following gases: A neon-helium mixture (90% Ne, 10 He), argon and pure helium. The helium distribution is shown in Fig. 15 and because helium's index is about ten times smaller than N_2 we obtain a much smaller ring. (Here the two lobes cannot be distinguished in the histogram due to insufficient resolution.) We also imaged fewer photons; hence, the need for a much longer run to obtain a reasonable statistical sample. However, the ring radius obtained from the fit should be accurate since the steep edges of the distribution largely determine the value for the radius. The result from our tests with argon was nearly identical to the N_2 result and the Ne - He result was similar to the He.

From the values of the ring radii obtained for the four gases, we were able to find a value of the index of refraction for each gas integrated over the photon energy range defined by our spectral acceptance.

We had

$$r = f \tan \theta$$

$$\cos \theta = 1/\beta n$$

using the fact that θ is small and $\beta \cong 1$ we used $\tan\theta \to \theta$, and obtain

$$\theta \approx \sqrt{2\left(1-\frac{1}{\beta n}\right)} \quad \text{and thus} \quad n-1 \approx \frac{1}{2}(r/f)^2 \quad .$$

We also noted $N = N_o L \sin^2\theta \approx N_o L \left(\frac{r}{f}\right)^2$

so:

$$\frac{n-1}{n} \approx \frac{1}{2} N_o L \quad = \text{constant independent of radiator gas (consistency check)}$$

Thus we obtained a rough value of the index of the refraction and a consistency check. We obtained the average number of photons per event by applying Poisson statistics to the value of the efficiency we obtained from the data

$e^{-N} = 1-\eta$, $\eta \equiv$ efficiency for getting one or more hits (photons) in the PWC for each particle passage.

N = average number of photons per particle passage.

The results for the above mentioned tests are summarized in Table 2. Note that our results agree fairly well with previous measurements except for our results with neon where no previous measurements could be found in the literature.

We also ran an O_2 contamination curve which is shown in Fig. 16. The slope of this line is linearly related to the absorption coefficient of O_2 in our acceptance region which is defined in the relation:

$I = I_o \exp(-kx)$, $k \equiv$ absorption coefficient

x = length of absorber

I = intensity detected

Table II

RESULT SUMMARY

a) Ring radius measurements, average number of photons detected

Gas	Radius (cm)	α	α(1216Å)*	Average Number of Photons Detected	α/N
N_2	3.7 ± 0.7	5.4 ± 0.2	5.71	0.34 ± 0.06	15.9 ± 2.9
Ar	3.6 ± 0.7	4.9 ± 0.2	5.65	0.39 ± 0.07	12.6 ± 2.3
He	1.1 ± 0.1	0.43 ± 0.08	0.427	0.043 ± 0.005	10.0 ± 2.2
Ne-He	1.5 ± 0.1	0.86 ± 0.10	--	0.057 ± 0.006	15.1 ± 2.4
Ne†	--	0.91 ± 0.20	--	--	--

$\alpha \equiv (n-1) \times 10^4$, where n is the index of refraction derived from our measurement of the ring radius.

*P. Gill and D.W.O. Heddle, J. Opt. Soc. Am. 53, 850 (1963)

†α for Ne obtained from the Ne-He data.

b) Absorption coefficient of O_2

$k = 17.0 \pm 2.0\ cm^{-1}$

We obtained a value of

$$k = 17.0 \pm 2.0 \text{ cm}^{-1} \quad .$$

Fig. 17 shows results for k over a large wavelength region done by previous researchers[5]. We note that our results are not grossly inconsistent with those shown in the figure.

We were not able to complete a quantitative pressure study but the few tests we did run with different pressures showed the expected variation of efficiency and ring size with pressure.

The result summary (Table 2) shows that the average number of photons detected per event for N_2 was 0.34 which is clearly far too low for any hope of imaging a ring in any single event. Therefore, we had to calculate the number of photons we expected, to see how much loss we could account for.

$$N = N_o L \sin^2\theta$$

$$N_o = \frac{\alpha}{\hbar c} \int_{E_1}^{E_2} \varepsilon_{mesh}(E)\ \varepsilon_{mirror}(E)\ \varepsilon_{LiF}(E)\ \varepsilon_{PI}(E)\ \varepsilon_{ABS}(E)\ dE$$

E_1, E_2 = the photon energy acceptance limits.

$\varepsilon_{PI}(E)$ = efficiency of photoionization and avalanche production.

$\varepsilon_{mesh}(E) \approx \varepsilon_{mesh} = 0.77$ (physical cross section measurement).

$\varepsilon_{ABS}(E)$ = transmission efficiency through the space from the LiF window to the active avalanche volume of the PWC due to finite cathode mesh thickness (absorption losses from CO_2 and benzene).

The various efficiency functions are plotted in Fig. 18. Note that these are all optimistic figures, i.e., values supplied by the manufacturer or in the case of ε_{PI}, taken from other researchers work. Each of these need to be measured for the components we used, but as yet we have no facility for measuring them.

Due to the benzene photoionization threshold on one end and the CO_2 absorption cutoff on the other, we assumed a useful energy range of 9.5 to 10.75 eV and then averaged the values for the efficiencies over that range. The value for N_o thus calculated was:

								N_o Estimate
N_o =	(370.)	(.77)	$(.70)^2$	(.5)	(.2)	(.80)	(1.25) = 14.0 cm^{-1}	Low
	(370.)	(.77)	$(.81)^2$	(.6)	(.5)	(.85)	(1.25) = 59.6 cm^{-1}	High
		mesh	mirrors	LiF	PI	ABS	(E_2-E_1)	

and hence

$$N = \begin{Bmatrix} 14.0 \\ 59.6 \end{Bmatrix} (96.5) (\sin 0.0324)^2$$

$$N \approx 1.4 \text{ to } 6.0 \text{ compare to } N_{actual} = 0.34$$

Clearly we are faced with a drastic loss of photons somewhere in the system. Our best guess at the reason for this problem of missing photons is that the amplifiers we employed were approximately 20 times less sensitive than state-of-the-art amplifiers; thus, we feel that a large portion of the photons created signals below the threshold of our discriminator. The loss of photons means that we were well below the knee of the single photon detection efficiency curve. We feel that this was the case because

we did see a continued increase in efficiency with increased voltage (although this increased voltage created larger cluster sizes for hits and subsequent breakdown occurrences). This theory of loss is further supported when looking at the results from the University of Michigan where they used amplifiers about ten times more sensitive than ours and were able to come within a factor of two of their expected number of photons. (They, however, were not imaging. Their results are summarized in the next section).

IV. Other Recent Results on Photoionization PWC's

1. Gilmore, et al.[2] (University of Bristol, Rutherford Lab.) using a device similar to ours, also imaged a Cerenkov ring with a one dimensional readout. Using argon as a radiator, they obtained a ring radius consistent with their expectations. From their efficiency they determined that they detected 0.63 photons per event compared to a calculated value of 7. In their paper they discuss a number of reasons why they observed many fewer photons than expected, and it is likely that they also may need more sensitive amplifiers.

2. Chapman, et al.[3] (University of Michigan) built a photoionizating PWC test device as a prototype for a threshold Cerenkov counter to be used in a PEP detector. They were not interested in imaging but their results with a threshold detector had significant bearing on the problems of an imaging detector. Using argon and N_2 as radiators, they made studies of detection efficiency versus pressure, versus benzene concentration, and versus radiator length. They observed 1.66 photons/event (1 atm N_2) versus an expected number of about 3.3. They, however, were using low noise FET input preamps which provided much greater sensitivity than our amplifiers;

even so, they feel that they do not yet have an optimum amplifier for the job. They also showed that there was about a 15% efficiency effect due to scintillation in argon but little or no effect in N_2.

V. Future Developments

If ring imaging is to be used in a large scale detector, the following topics will need investigation:

1. PWC gas mixtures (to obtain stability and optimum quantum efficiency).
2. Two-dimensional readout schemes.
3. State-of-the-art amplifiers.
4. Thin film windows (in place of the expensive LiF and Mg_2F crystal windows).
5. Exotic photoionization gases (such as triethylamine, TMAE, etc., which have yet to be tried in a detection device).
6. Chamber lifetime studies (which are important because of the new gas mixtures).
7. New detector geometries and new type detectors (needle chambers, drift chambers).

Our group, as well as several others we have heard from, are planning research in these important areas.

VI. Conclusions

We have shown that one can use the photoionization technique to obtain an image of the Cerenkov ring. Argon, N_2, neon and helium have been tested and shown to function well as radiator media. The results for the ring radii

obtained agree with previous measurements of the VUV index of refraction and we also obtained a value for the O_2 absorption coefficient averaged in our photon energy range. The outstanding problem, however, was the disparity between the number of photons observed and the number expected. With direct measurement of the transmissions, reflectances, and efficiencies of the various components, and with the use of more sensitive amplifiers, we hope to be able to account for the difference.

VII. Acknowledgment

We would like to thank Al Kilert, Bill Walsh and Don McShurley for their excellent technical support, Ted Fieguth for helping us with the beam line, Steve Shapiro for his help with our electronics, and John Malos, who worked with us in the early developmental stages of this project.

REFERENCES

1. J. Sequinot and T. Ypsilantis, Nucl. Inst. and Meth. 142, 377-391 (1977).
2. Gilmore, et al., Print - 78-0705 (Rutherford), July 1978, 12 pp.
3. J. Chapman, et al., UM HE 78-23 HRS 37 (1978)
4. A. Etkin, et al., Proc. Of Isabelle Summer Workshop (1977) pp. 72-77.
5. R. Watanabe, et al., J. Chem. Phys. 21, 1026 (1953).

FIGURE CAPTIONS

1. Schematic large phase space acceptance Cerenkov ring imaging detector (from Ref. 1).
2. Example of Cerenkov ring radius versus momentum for pions, kaons, and protons.
3. Example of the accuracy of momentum measurement using the Cerenkov ring radius for pions (a), kaons (b), and protons (c). $N_o = 74$, L = 100 cm, f = 100 cm, Δr = 2 mm, $n-1 = 5.7 \times 10^{-4}$.
4. Ionization thresholds and window cutoffs for various materials (from Ref. 4).
5. Schematic photoionizing needle chamber (from Ref. 1).
6. Cerenkov radiator tube cross section.
7. Cerenkov ring imaging proportional wire chamber.
8. Trigger logic.
9. Schematic of data acquisition system.
10. Chamber efficiency plateau (a) Ar, CO_2, benzene, (b) magic gas.
11. Clustered argon distribution with a 4 cm mask over window.
12. (a,b,c) Expected distributions for rings imaged in one dimension.
13. Clustered corrected nitrogen distribution.
14. Offset nitrogen distribution.
15. Clustered corrected helium distribution.
16. Oxygen contamination curve.
17. Absorption coefficient of O_2 in the region 1050-1300Å (from Ref. 5).
18. Device component efficiencies in vacuum ultraviolet: A--transmission through benzene and CO_2 before mesh; B--mirror reflectance; C--Lif transmission; D--benzene photoionization efficiency.

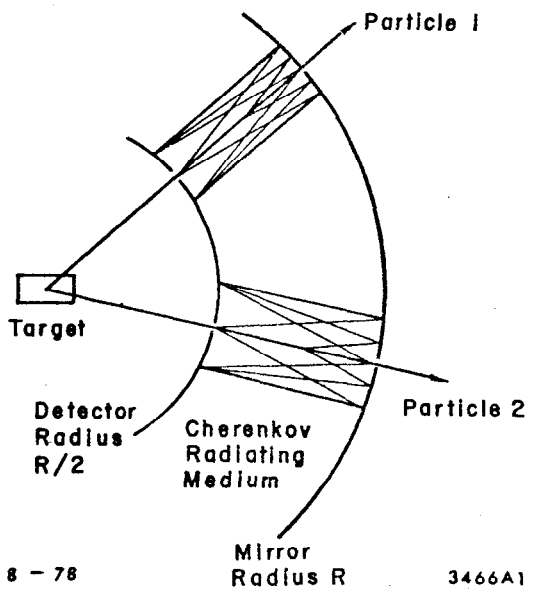
Particle 1
Target
Particle 2
Detector
Radius
R/2
Cherenkov
Radiating
Medium
Mirror
Radius R
8 – 78
3466A1

Fig. 1

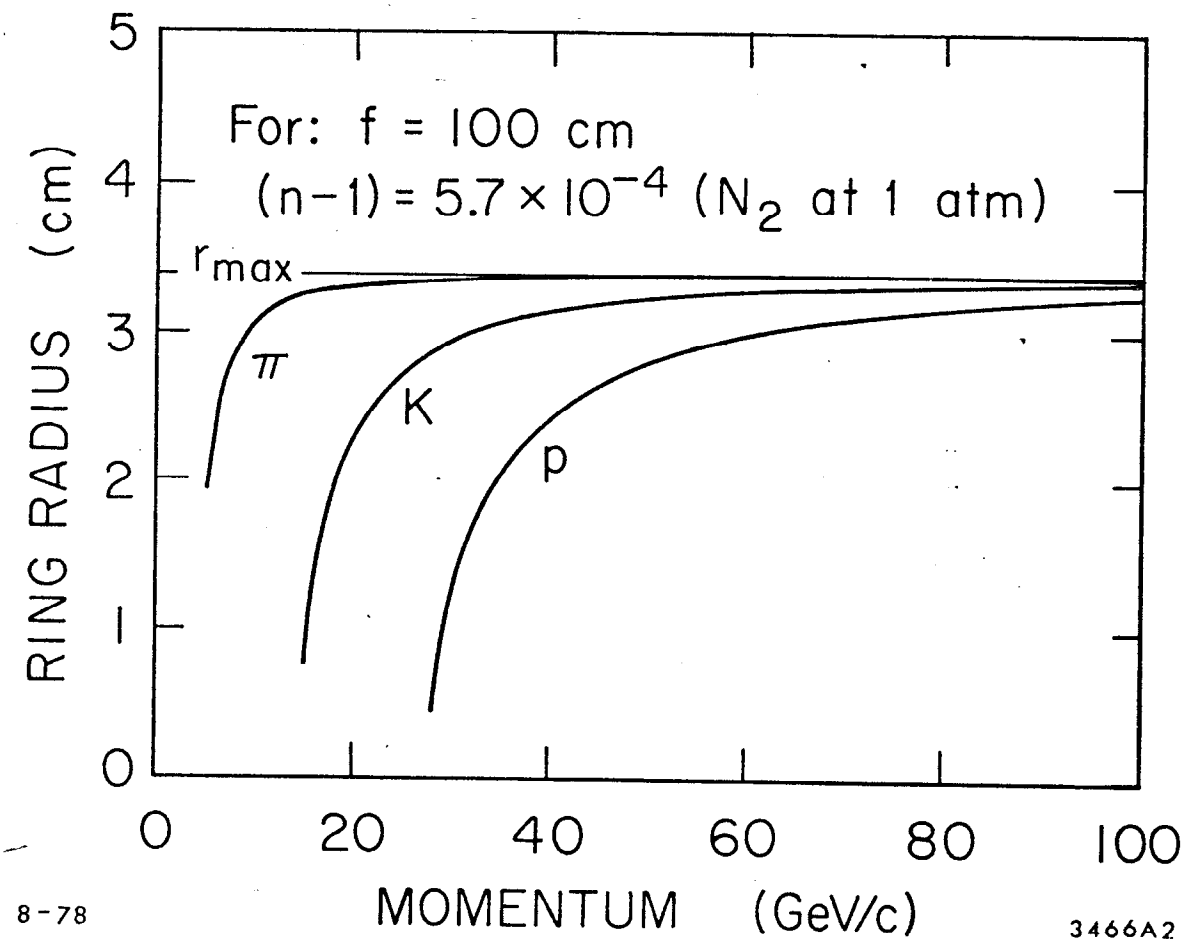
For: f = 100 cm
(n-1) = 5.7 × 10⁻⁴ (N₂ at 1 atm)
r max
π
K
p
RING RADIUS (cm)
MOMENTUM (GeV/c)
0
1
2
3
4
5
0
20
40
60
80
100
8-78
3466A2

Fig. 2

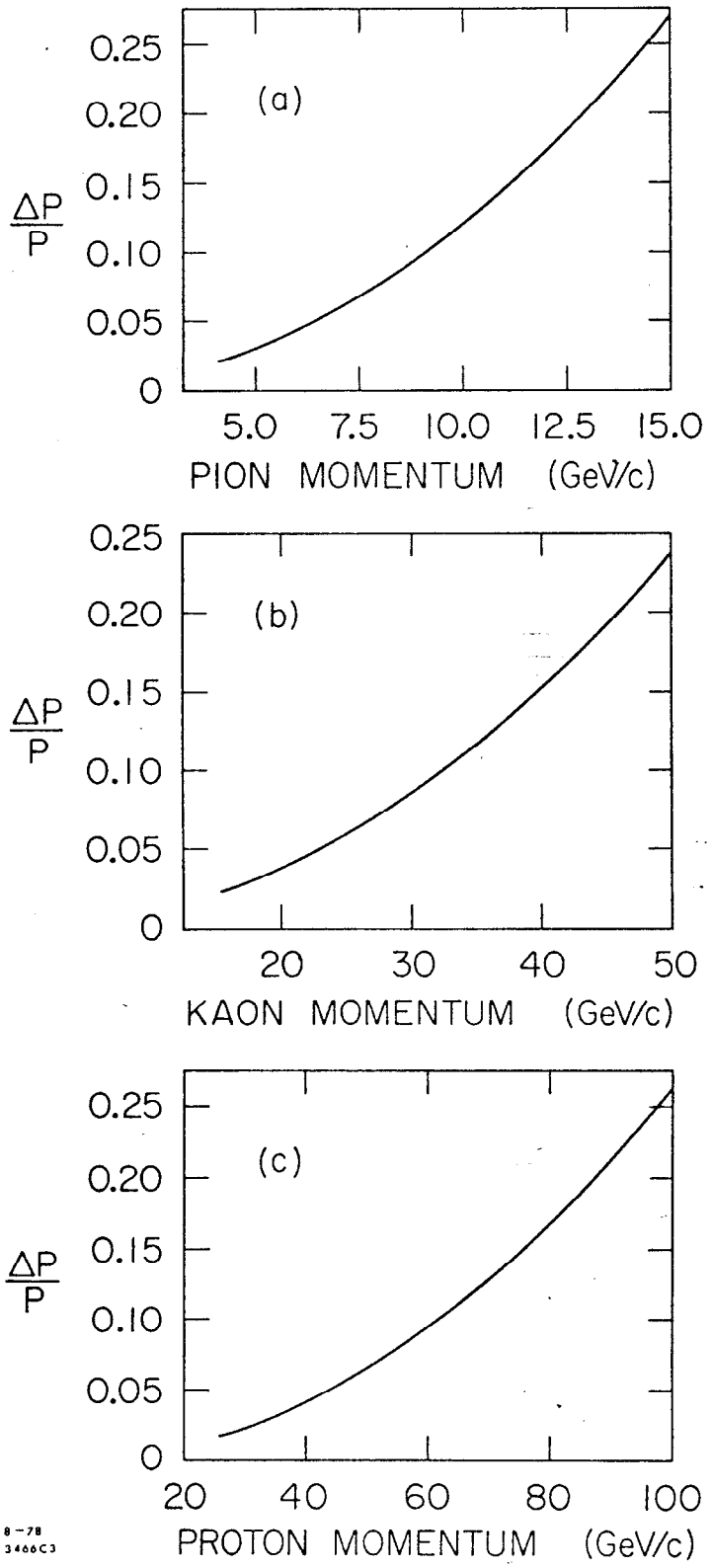
(a)
0.25
0.20
0.15
0.10
0.05
0
ΔP/P
5.0
7.5
10.0
12.5
15.0
PION MOMENTUM (GeV/c)
(b)
20
30
40
50
KAON MOMENTUM (GeV/c)
(c)
20
40
60
80
100
PROTON MOMENTUM (GeV/c)
8-78
3466C3

Fig. 3

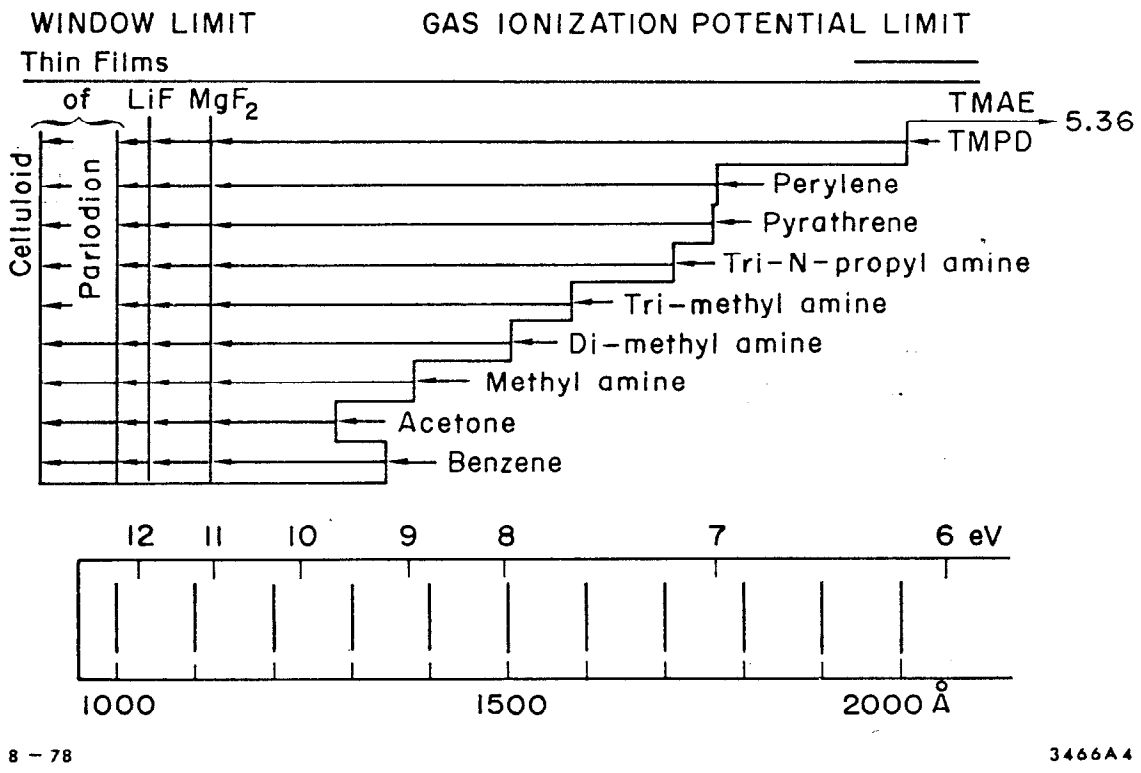
WINDOW LIMIT
GAS IONIZATION POTENTIAL LIMIT
Thin Films
of
LiF
MgF_2
Celluloid
Parlodion
TMAE
5.36
TMPD
Perylene
Pyrathrene
Tri-N-propyl amine
Tri-methyl amine
Di-methyl amine
Methyl amine
Acetone
Benzene
12
11
10
9
8
7
6 eV
1000
1500
2000 Å
8 - 78
3466A4

Fig. 4

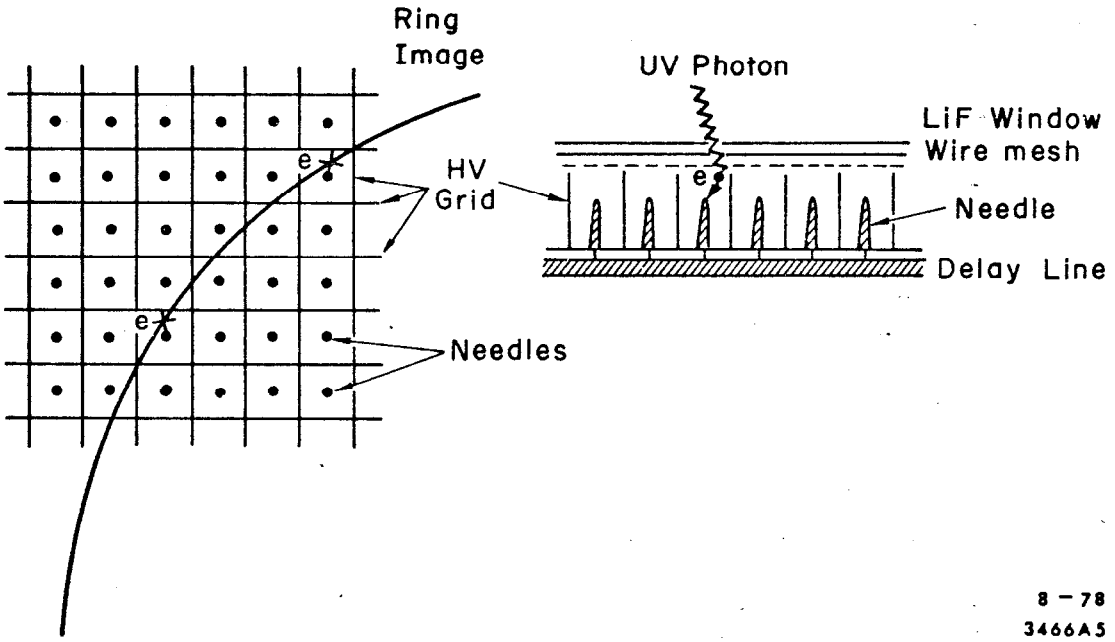
Ring
Image
UV Photon
LiF Window
Wire mesh
HV
Grid
e
e
Needle
Delay Line
Needles
8 – 78
3466A5

Fig. 5

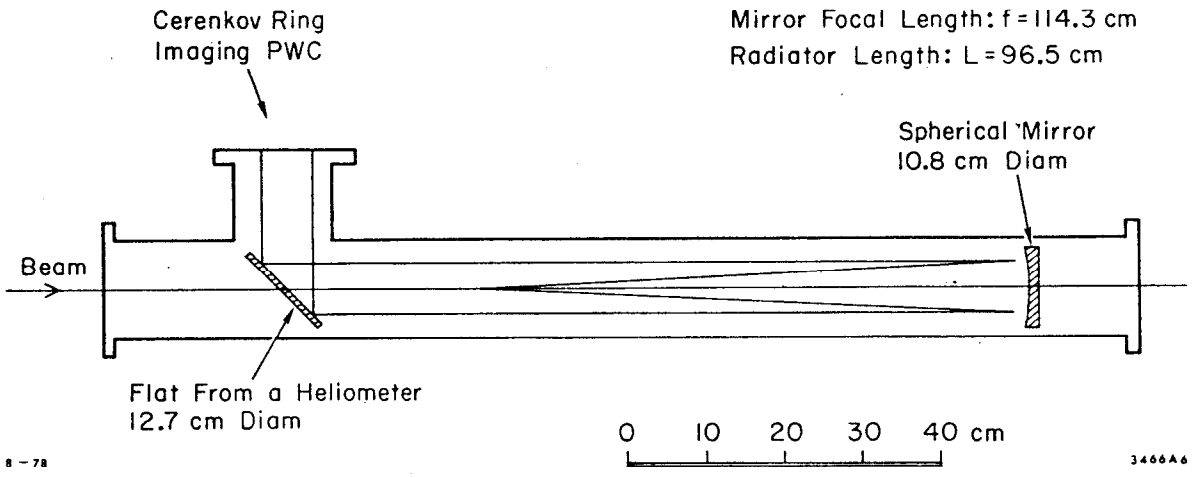
Cerenkov Ring
Imaging PWC
Mirror Focal Length: f = 114.3 cm
Radiator Length: L = 96.5 cm
Spherical Mirror
10.8 cm Diam
Beam
Flat From a Heliometer
12.7 cm Diam
0 10 20 30 40 cm
8-78
3466A6

Fig. 6

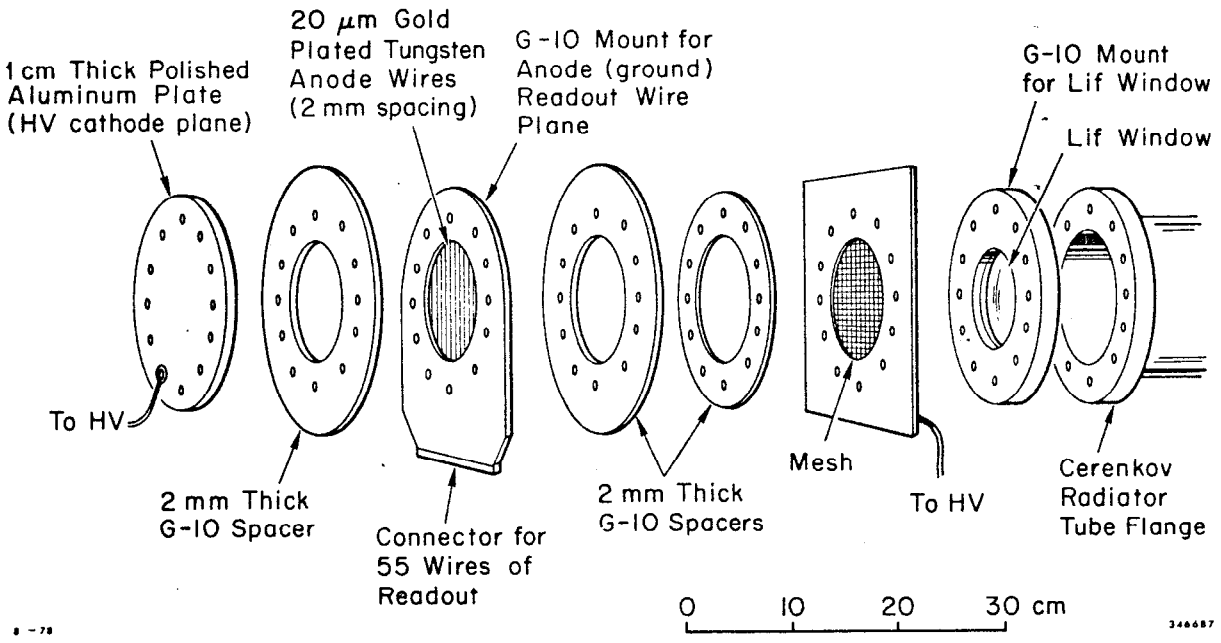
1 cm Thick Polished
Aluminum Plate
(HV cathode plane)
20 μm Gold
Plated Tungsten
Anode Wires
(2 mm spacing)
G-10 Mount for
Anode (ground)
Readout Wire
Plane
G-10 Mount
for Lif Window
Lif Window
To HV
2 mm Thick
G-10 Spacer
Connector for
55 Wires of
Readout
2 mm Thick
G-10 Spacers
Mesh
To HV
Cerenkov
Radiator
Tube Flange
0
10
20
30 cm

Fig. 7

TRIGGER LOGIC

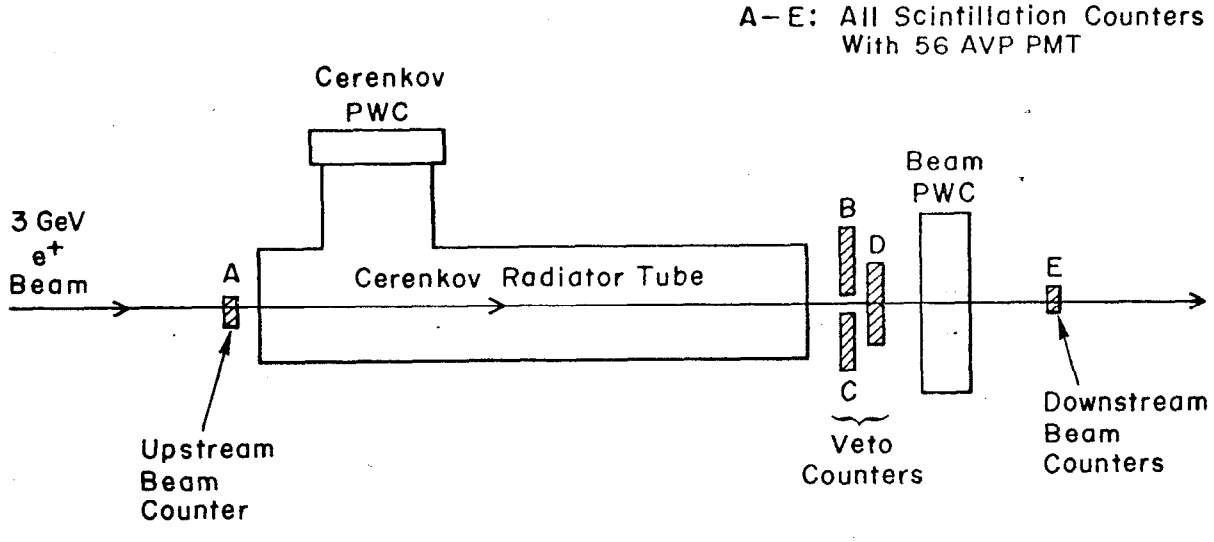

8-78

$$\text{Event} = A \cdot \bar{B} \cdot \bar{C} \cdot \bar{D} \cdot E \cdot (\text{Beam Spill}) \cdot (\text{LSI Ready})$$

3466A8

Fig. 8

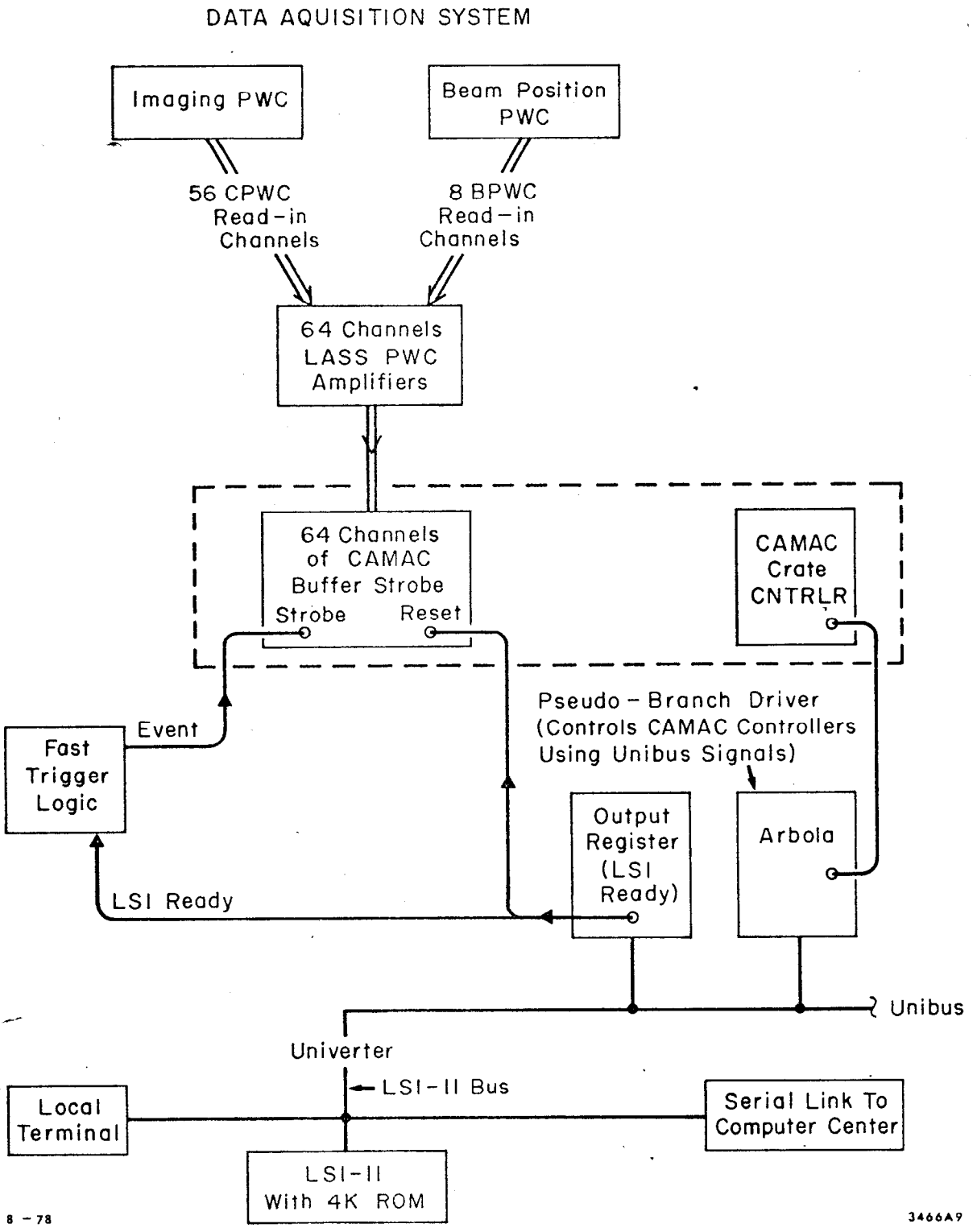
DATA AQUISITION SYSTEM
Imaging PWC
Beam Position PWC
56 CPWC Read-in Channels
8 BPWC Read-in Channels
64 Channels LASS PWC Amplifiers
64 Channels of CAMAC Buffer Strobe
Strobe
Reset
CAMAC Crate CNTRLR
Pseudo-Branch Driver (Controls CAMAC Controllers Using Unibus Signals)
Event
Fast Trigger Logic
Output Register (LSI Ready)
Arbola
LSI Ready
Unibus
Univerter
LSI-11 Bus
Local Terminal
Serial Link To Computer Center
LSI-11 With 4K ROM
8 - 78
3466A9

Fig. 9

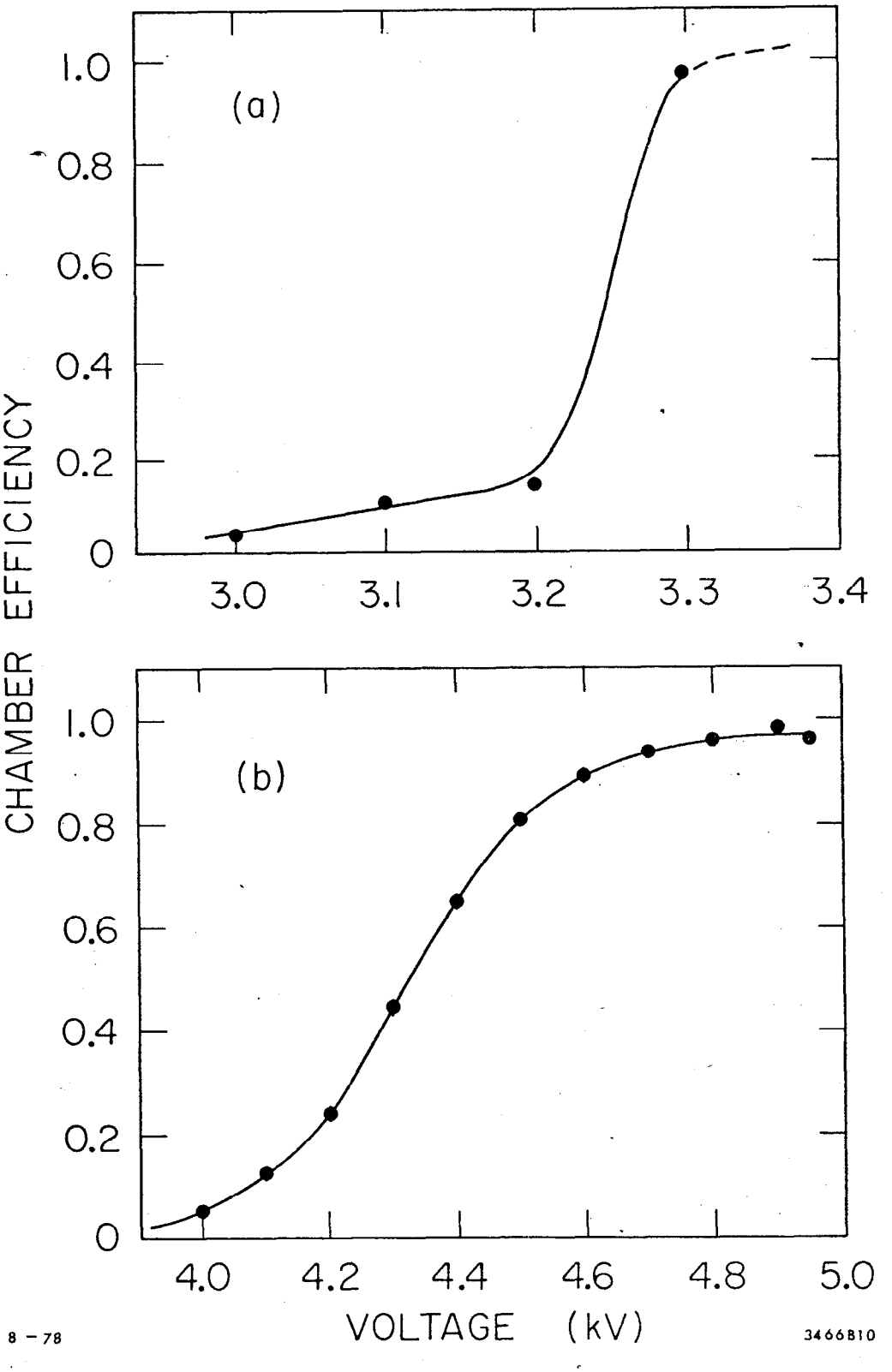
(a)
(b)
CHAMBER EFFICIENCY
1.0
0.8
0.6
0.4
0.2
0
3.0
3.1
3.2
3.3
3.4
4.0
4.2
4.4
4.6
4.8
5.0
VOLTAGE (kV)
8 - 78
3466B10

Fig. 10

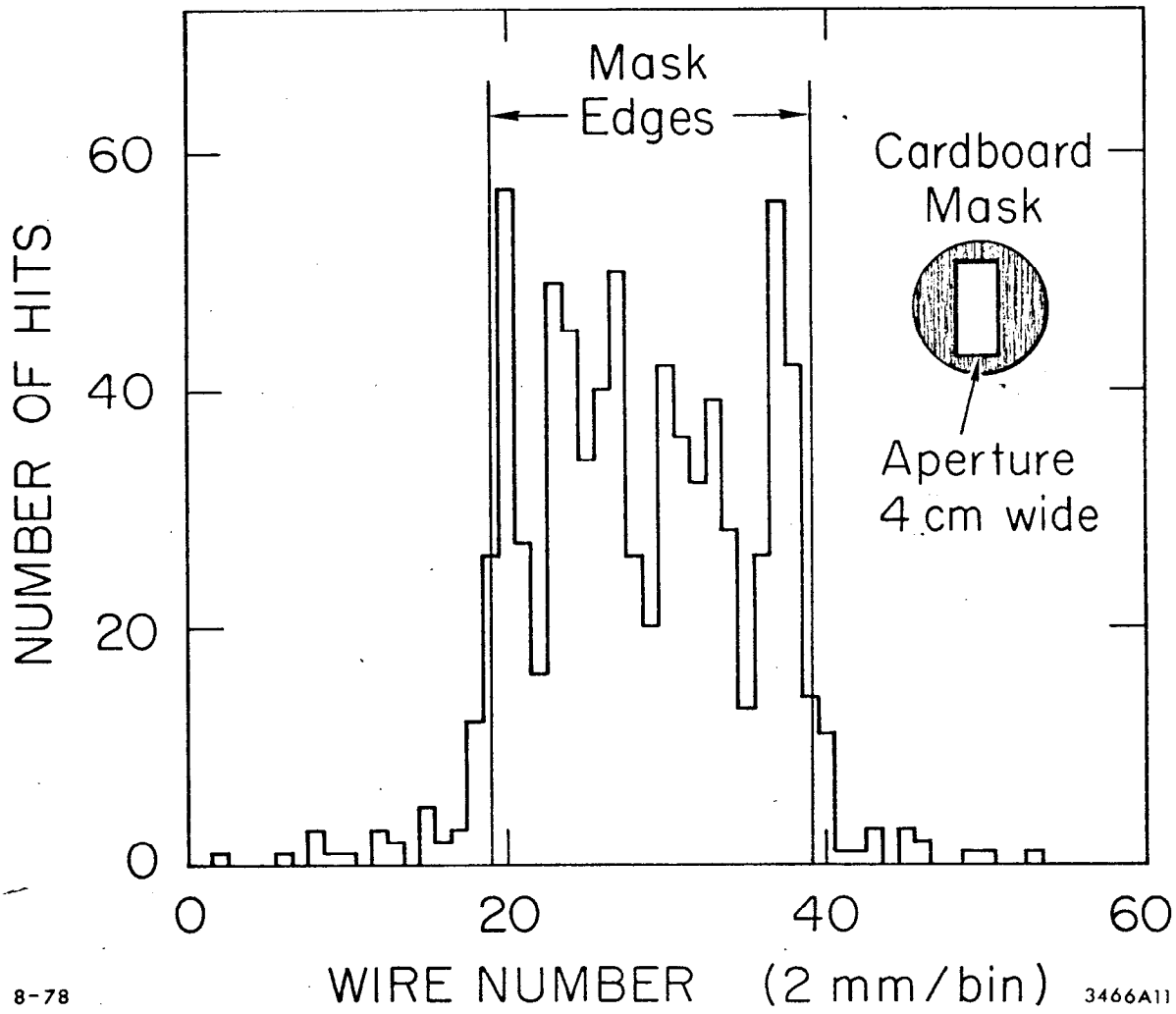
Mask
Edges
Cardboard
Mask
Aperture
4 cm wide
NUMBER OF HITS
0
20
40
60
0
20
40
60
WIRE NUMBER (2 mm/bin)
8-78
3466A11

Fig. 11

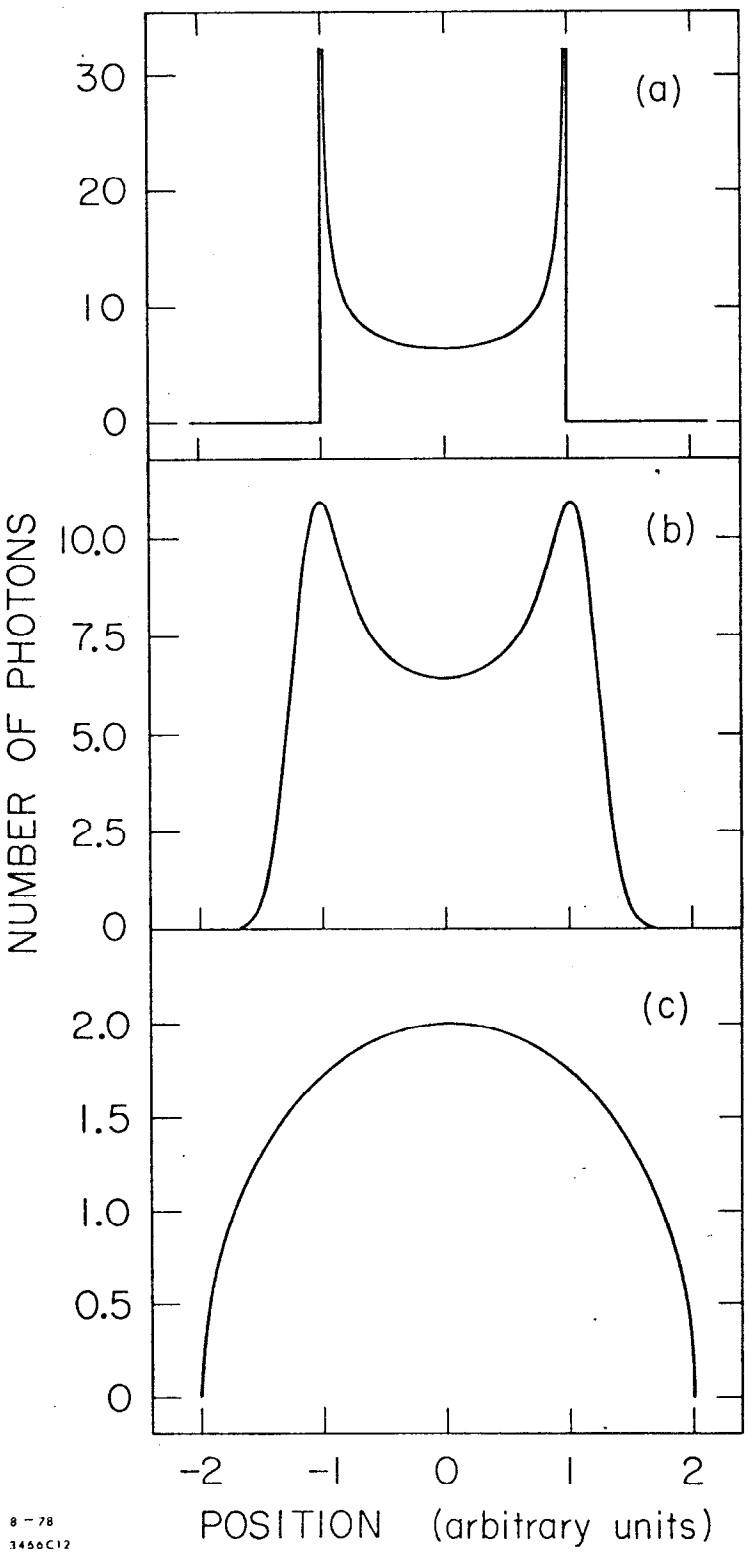
30
20
10
0
(a)
10.0
7.5
5.0
2.5
0
(b)
NUMBER OF PHOTONS
2.0
1.5
1.0
0.5
0
(c)
-2
-1
0
1
2
POSITION (arbitrary units)
8-78
3456C12

Fig. 12

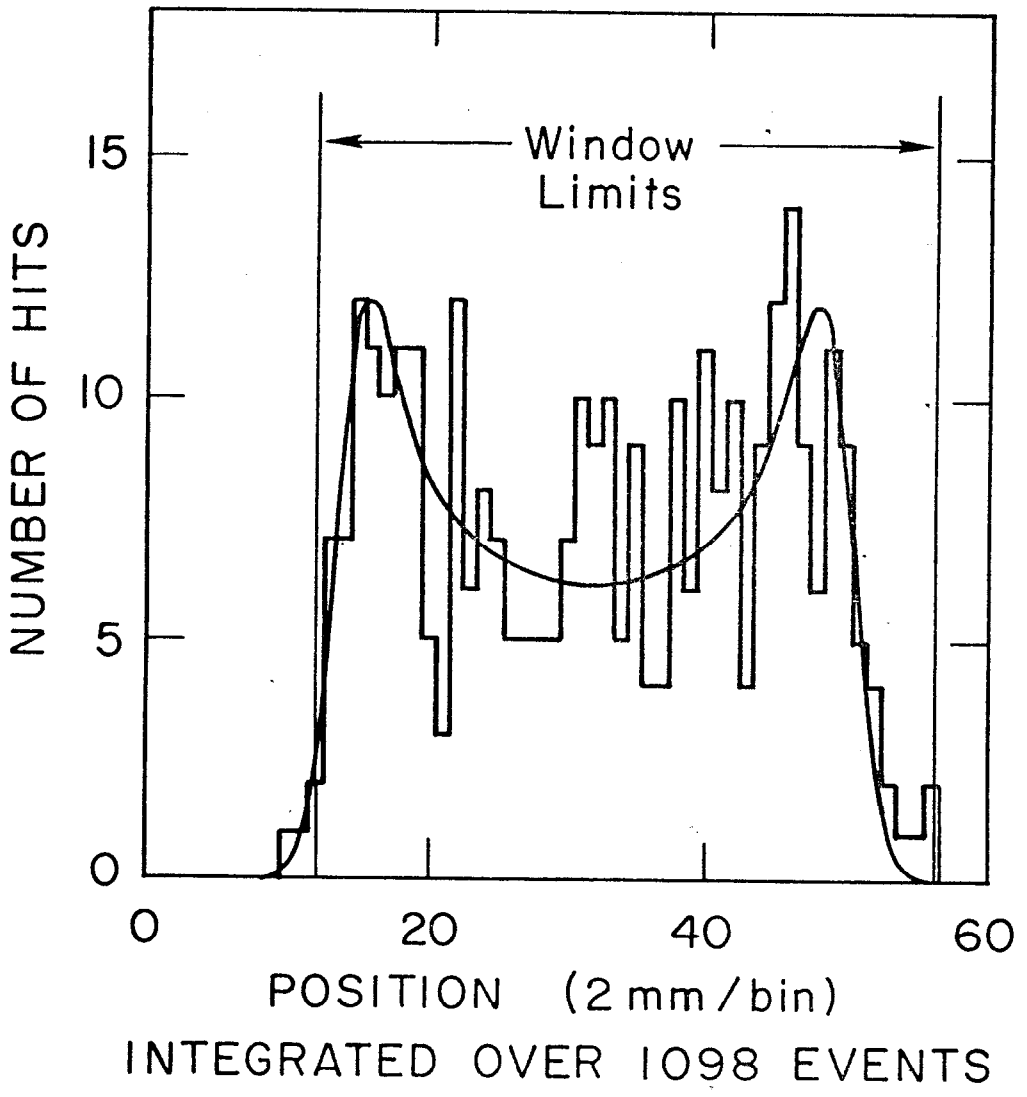
Window
Limits
NUMBER OF HITS
15
10
5
0
0
20
40
60
POSITION (2 mm / bin)
INTEGRATED OVER 1098 EVENTS
8 - 78
3466A13

Fig. 13

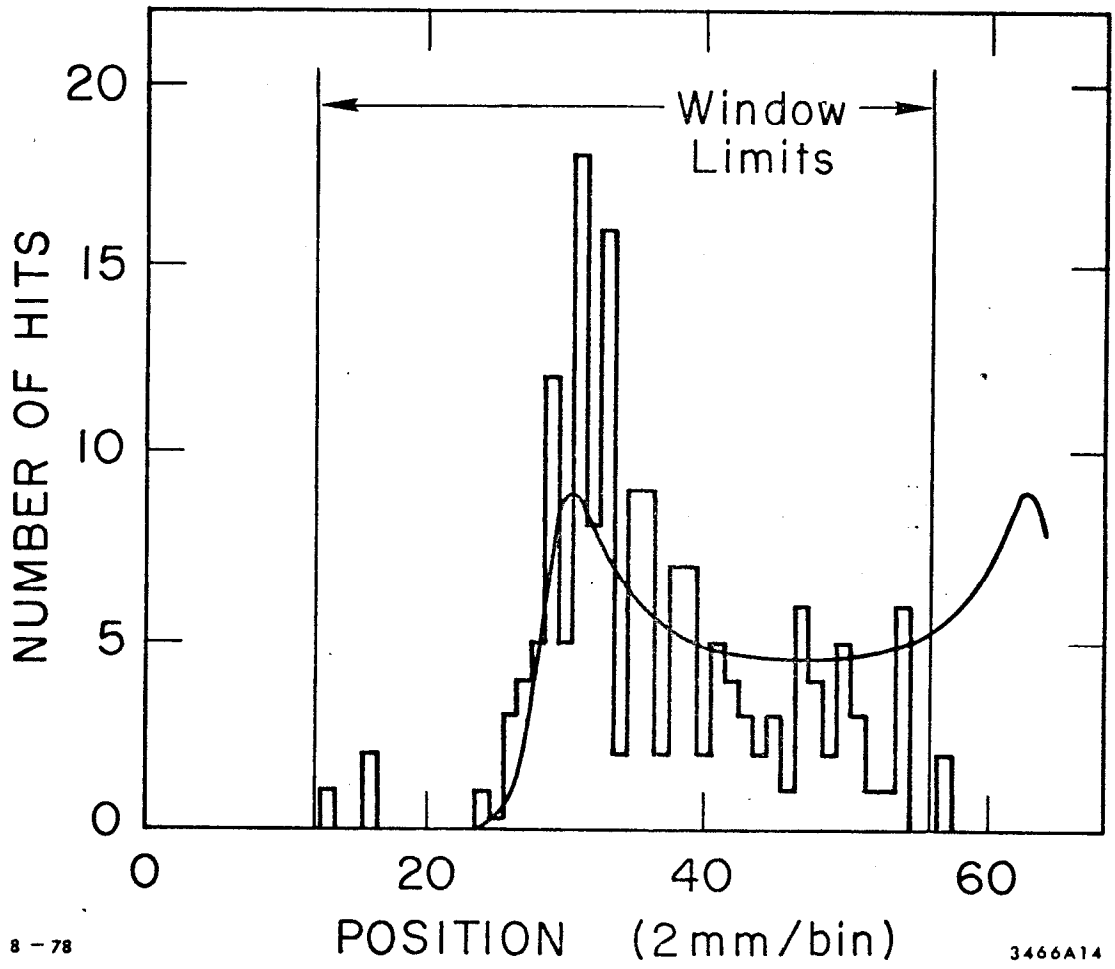
20
15
10
5
0
NUMBER OF HITS
Window
Limits
0
20
40
60
POSITION (2mm/bin)
8-78
3466A14

Fig. 14

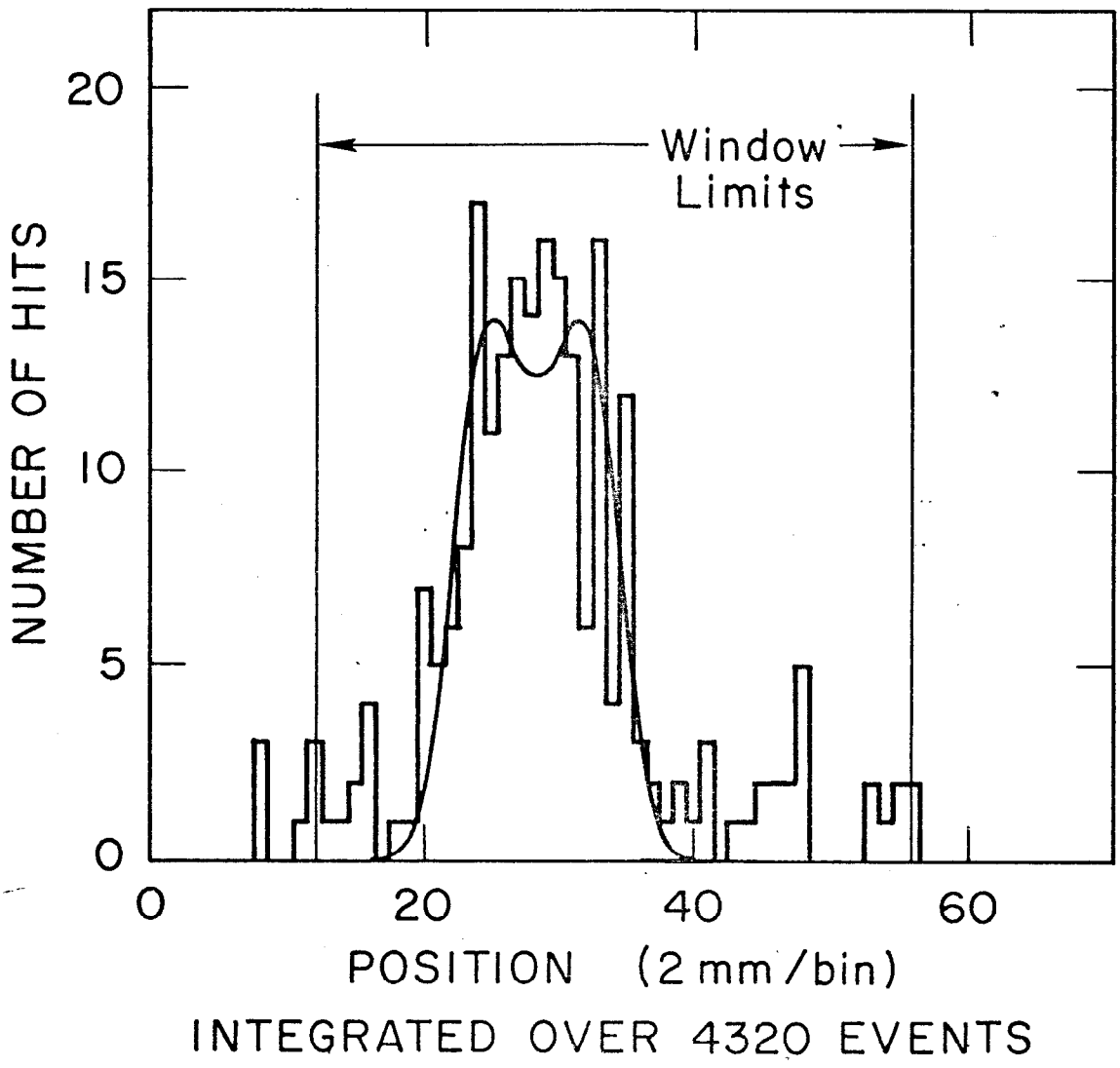
20
15
10
5
0
NUMBER OF HITS
Window
Limits
0
20
40
60
POSITION (2 mm/bin)
INTEGRATED OVER 4320 EVENTS
8 – 78
3466A15

Fig. 15

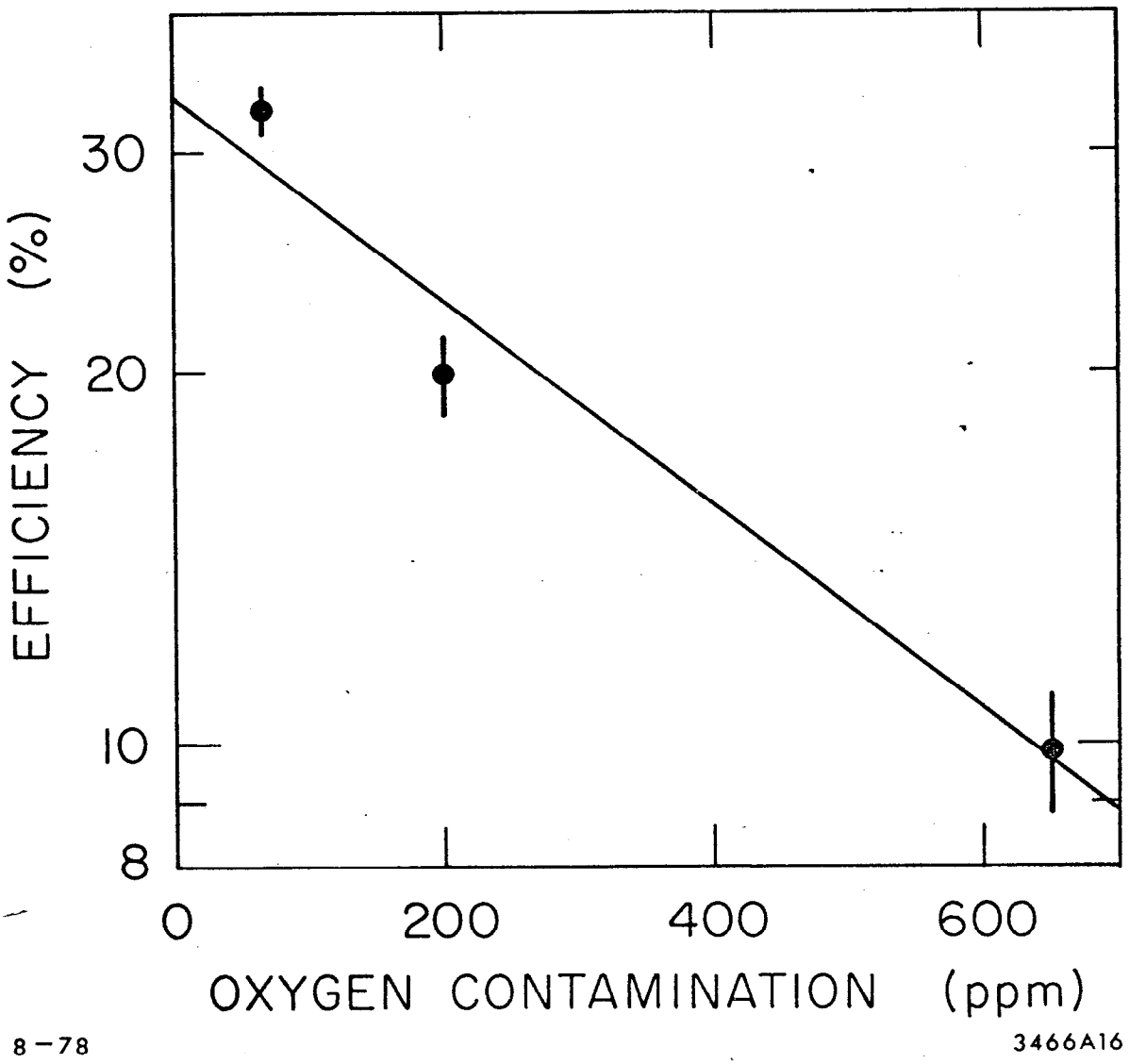
EFFICIENCY (%)
30
20
10
8
0
200
400
600
OXYGEN CONTAMINATION (ppm)
8-78
3466A16

Fig. 16

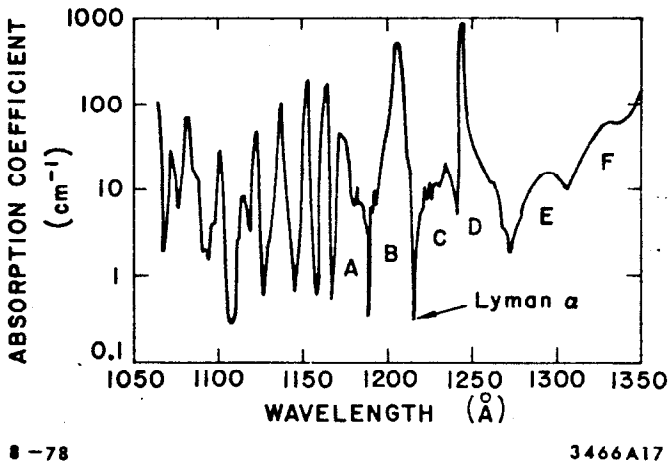
ABSORPTION COEFFICIENT (cm⁻¹)
1000
100
10
1
0.1
A
B
C
D
E
F
Lyman α
1050
1100
1150
1200
1250
1300
1350
WAVELENGTH (Å)
8-78
3466A17

Fig. 17

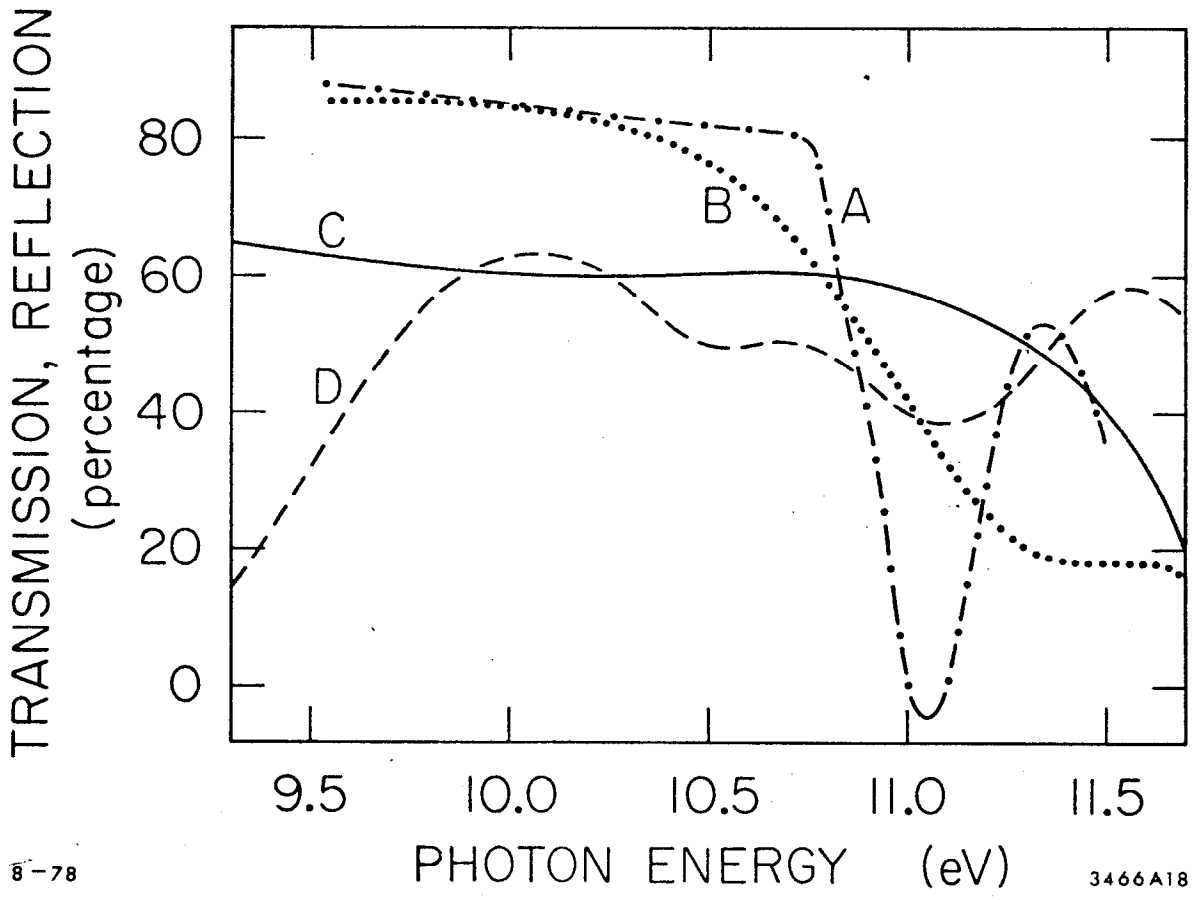
TRANSMISSION, REFLECTION
(percentage)
80
60
40
20
0
A
B
C
D
9.5
10.0
10.5
11.0
11.5
PHOTON ENERGY (eV)
8-78
3466A18

Fig. 18